

# Molecular Dynamics of a Liquid Crystalline Polymer Studied by Two-Dimensional Fourier Transform and CW ESR

Dajiang Xu, Richard H. Crepeau, Christopher K. Ober,<sup>†</sup> and Jack H. Freed\*

*Baker Laboratory of Chemistry, Cornell University, Ithaca, New York 14853-1301*

*Received: February 16, 1996; In Final Form: May 20, 1996*<sup>⊗</sup>

Two-dimensional Fourier transform (2D-FT) and CW-ESR experiments at X-band frequencies were performed over a broad range of temperatures covering the solid and melt states of a liquid crystalline (LC) polymer. The CW-ESR experiments were analyzed by conventional motional models. The nematic phase was macroscopically aligned in the dc magnetic field, whereas the solid state showed microscopic order but macroscopic disorder (MOMD). An end-label on the polymer showed smaller ordering and larger reorientational rates than that of the cholestane (CSL) spin probe dissolved in the same polymer, since the former can reorient by local internal chain modes. It was demonstrated that the 2D-FT-ESR experiments provide greatly enhanced resolution to the ordering and dynamics of the end-label, especially when performed as 2D-ELDOR (electron–electron double resonance) experiments as a function of mixing time. The conventional model of Brownian reorientation in an orienting potential was unsuccessful in interpreting these results. Instead the model of a slowly relaxing local structure (SRLS), which enables differentiation between the local internal modes experienced by the end-label and the collective reorganization of the polymer molecules around the end label, yielded much improved fits to the experiments in the nematic phase. These nonlinear least squares fits showed that the polymer “cage” relaxes more than 2 orders of magnitude slower than the local end-chain modes, and there is a moderate orientational potential coupling the local end-chain motion to the “cage” with axial and nonaxial local order parameters of about 0.14 and 0.29 at 100 °C. In the solid state the 2D-ELDOR spectra were fitted to the MOMD model, which is a limiting case of the SRLS model when the cage relaxation becomes very slow.

## 1. Introduction

Electron spin resonance (ESR) has been extensively applied in the study of molecular structure and dynamics in isotropic fluids, ordered phases such as liquid crystals, and lipid model membranes<sup>1,2</sup> as well as for polymers.<sup>3,4</sup> The high sensitivity and favorable time scale of ESR have made it a powerful tool for studying both the microscopic ordering and the molecular dynamics. We have been interested in extending this ESR approach to study liquid crystalline (LC) polymer systems. Due to the complex nature of LC polymers, the interpretation of the ESR spectra may be expected to require sophisticated dynamic models and spectral simulations, although simple analyses were utilized in previous ESR studies on different LC polymers.<sup>5,6</sup>

For many polymeric LC systems it is not conveniently possible to prepare macroscopically well-aligned samples that can provide enhanced spectral resolution and orientation dependence. In most cases, the “dispersed” MOMD (microscopically ordered but macroscopically disordered) sample, whose ESR spectrum can be approximated as the superposition of spectra from microscopically well-ordered local domains that are randomly oriented, may readily be prepared. Despite the limited spectral resolution and substantially increased computing time required in the simulation, ESR has played a useful role in extracting dynamic and structural information from such MOMD spectra.<sup>7</sup>

In a companion paper, we describe a CW-ESR study on a thermotropic main chain LC polymer model system, end labeled by a nitroxide free radical, in its nematic phase.<sup>8</sup> We have found some of these samples were macroscopically aligned by the ESR magnetic field of 3.3 kG, while some of them could be

characterized as MOMD, and some showed a mixture of these two kinds of spectra. The degree of macroscopic alignment was shown to be largely dependent upon the molecular weight of the matrix molecules in which the labeled ones were dissolved; the lower the molecular weight, the more readily it is aligned.

In that work it was found that in the nematic phase the reorientational motion probed by the end-labeled nitroxide was sensitive to the matrix molecular weight but not to that of the spin-labeled tracer molecule. In the present paper we examine the thermal behavior of the same main chain LC polymer system. We utilized both the 3-carboxy-PROXYL spin label attached to the LC polymer and, in the case of our CW-ESR studies, the rigid CSL probe as a solute. It is known that CSL reports on the overall ordering of the solvent molecules,<sup>9</sup> whereas the spin label on the end of the chain reflects the combined motion of the backbone, its internal modes, and the flexible bond between the backbone and the label.<sup>10</sup> Our initial experiments reported here were by standard CW-ESR as in ref 8. However, it is now conveniently possible to employ modern two-dimensional Fourier transform (2D-FT) ESR methods to study the motional dynamics in these systems, as we show in the present study.

An important recent development in ESR spectroscopy has been that of 2D-FT-ESR.<sup>11–15</sup> This development has the technical advantages of (a) greatly reduced data acquisition times, because the whole spectrum is irradiated simultaneously (i.e. the multiplex advantage) with the use of very narrow nonselective pulses (widths  $\sim 5$  ns) that are significantly shorter than the relevant  $T_2$ 's. As a result they yield (b) reduced dead time and less spectral distortion than what arises from the use of long pulses. More important is the availability of a whole class of new experiments to study both motion and structure.

<sup>†</sup> Dept. of Materials Science and Engineering, Cornell University, Ithaca, NY 14853.

<sup>⊗</sup> Abstract published in *Advance ACS Abstracts*, September 1, 1996.

We wish to distinguish this important technique of 2D-FT-ESR from other recent and important 2D-ESR methods, which however lack the multiplex advantage in that neither the echo decay nor the free induction decay is collected, nor does one attempt to irradiate the full spectrum, since selective microwave pulses are used.<sup>16</sup> These methods have primarily been in the class of electron spin echo modulation (ESEEM) experiments, which emphasize structural studies,<sup>13,15,17,18</sup> but they also include studies of very slow motional dynamics.<sup>13,14</sup> While modern 2D-FT-ESR can provide the multiplex advantage and an additional spectral dimension to ESEEM studies as described elsewhere,<sup>16</sup> we focus here on its use for dynamic studies. The early 2D-FT-ESR work of Freed and co-workers emphasized the study of translational diffusion by Heisenberg exchange<sup>11,12</sup> and rotational diffusion by modulation of the hf tensor,<sup>19</sup> leading to cross-peak generation. Bowman<sup>15</sup> showed how the cross-peaks can be used to study intermolecular chemical exchange, whereas Goldfarb and co-workers<sup>20</sup> demonstrated its use for slow intramolecular chemical exchange. More recently, Dinse<sup>21</sup> has demonstrated its potential for the investigation of transient radicals. All of these applications involve motionally narrowed ESR spectra.

Our present study, however, addresses slow motional and near rigid limit spectra, which provide the additional challenges of wide spectral bandwidth, very short (inhomogeneous)  $T_2^*$ 's and usually very short (homogeneous)  $T_2$ 's. Recent developments have now made it possible to study such cases by modern 2D-FT-ESR methods.<sup>16,22–24</sup> These 2D-FT-ESR spectra provide enhanced resolution to dynamic molecular structure compared to conventional CW-ESR spectra, especially those that are inhomogeneously broadened by the macroscopic disorder. Recent studies have illustrated the great potential of slow motional 2D-FT-ESR for the study of complex fluids.<sup>23,24</sup> The model LC polymer system<sup>8</sup> used in our present work has many similarities to complex fluids, which are characterized by slower motion and very short  $T_2^*$ 's, due partly to the inhomogeneities of MOMD. In CW-ESR spectra, it is difficult to distinguish this inhomogeneous MOMD broadening effect from the homogeneous line broadening (which arises mainly from the rotational modulation of hyperfine (hf) and  $g$  tensors) and from other inhomogeneous broadening (e.g. from proton super-hyperfine (shf) interactions). Previous study has shown how 2D-FT-ESR methods enable one to obtain the details of the complex spin relaxation processes in lipid membranes<sup>23,24</sup> and in a single crystal.<sup>16</sup> With significant improvements in capabilities of instrumentation, including shortened spectrometer dead times, enhanced signal to noise resulting from very rapid signal averaging of successive pulse sequences, and improved data processing and filtering, it is now feasible to perform 2D-FT-ESR experiments on liquid crystalline polymers to obtain high-quality 2D-FT-ESR spectra. Using the well-developed theory for the analysis of 2D-FT-ESR spectra,<sup>25,26</sup> we are able to perform nonlinear least squares (NLLS) fitting of sets of 2D-FT-ESR spectra to quantify the details of molecular ordering and dynamics as a function of temperature.

We report here the first 2D-FT-ESR study of a nitroxide spin-labeled LC polymer. We illustrate its capabilities by comparison with our CW-ESR studies of the same class of LC polymer. The primary objective of the present work is to relate the phase behavior of LC polymers to the ordering and dynamic information available from 2D-FT- and standard CW-ESR techniques. Our methods provide a general approach for learning about anisotropic rotational diffusion, orientational ordering, and local domain or cage structure.

The now standard CW-ESR spectral analysis has been discussed in detail elsewhere.<sup>1,26–29</sup> Spectral simulation of experiments based on the stochastic Liouville equation (SLE) utilizing a nonlinear least squares (NLLS) fitting algorithm has been performed to obtain the dynamic and ordering information in the slow motional regime from both macroscopically aligned and MOMD samples.<sup>7,27</sup> Recent improvements in this approach, which includes applying the “model trust region” modification of the Levenberg–Marquardt minimization algorithm, have greatly increased the efficiency of the fitting procedure and have several other useful features.<sup>26</sup> Thus, it also includes a separation-of-variables method to deal more effectively with the linear coefficients, and it allows fitting to multicomponent spectra. We could also take advantage of this modified “user-friendly” program to perform interactive, real-time NLLS fitting on a laboratory workstation with a graphical interface. Such improved features have enabled us to perform NLLS fitting in a very efficient and reliable manner to study by ESR methods the dynamics of LC polymeric samples over a broad temperature range.

The analysis of the 2D-FT-ESR spectra, while less familiar, proceeds in a manner analogous to (but more complex than) that of CW-ESR spectra.<sup>25</sup> We utilize NLLS fitting of solutions of the SLE to sets of 2D spectra obtained as a function of mixing time (which actually provides a third “spectral” dimension).<sup>23,24,26</sup> We find that the increased resolution to ordering and dynamics provided by these “extra spectral dimensions” cannot be adequately fit by the standard models of motional dynamics.<sup>28–30</sup> This is especially clear for the nematic phase.

Recently, Polimeno and Freed have developed the slowly relaxing local structure (SRLS) model of solvent cage effects to interpret the slow motional ESR spectra obtained from complex fluids.<sup>31</sup> The SRLS model describes the molecular motion in terms of the reorientation of the spin-labeled probe molecule within a dynamic solvent cage that reorients on a slower time scale. Whereas both the probe molecule and the cage can experience microscopic aligning potentials, there is an additional potential describing the coupling between the probe and the cage. Thus the motion of the probe is described by the same set of parameters as simple Brownian reorientation, while the cage, which is a set of collective parameters that represent the instantaneous solvent structure around the probe, is also described as a Brownian rotor. That is, the SRLS model consists of two coupled Brownian rotors. This SRLS model is in fact supported by recent molecular dynamics simulations on a simple liquid.<sup>32</sup> This SRLS model has been incorporated into the SLE in a form that enables NLLS fitting to experimental spectra,<sup>31</sup> and significant improvements were found in fitting 250 GHz CW-ESR spectra of spin probes dissolved in a glass-forming solvent, when compared to the model of simple Brownian reorientation.<sup>31</sup> This SRLS model has now been incorporated into the NLLS fitting programs for 2D-FT-ESR,<sup>33</sup> and it has led to improved fitting of 2D-ESR spectra from spin probes dissolved in a macroscopically aligned thermotropic liquid crystal (nonpolymeric).<sup>33</sup>

Just as the standard Brownian model (in an orienting potential when needed) has been so effective in interpreting CW-ESR spectra for so many years, one may expect that an improved model, such as the SRLS model, would have a more general applicability to a wide range of systems, when studied by modern ESR spectroscopies yielding improved resolution to molecular dynamics. In the case of the LC polymer that is end labeled, one can regard the local motion of the probe including the internal motion of the chain to which it is attached, as well as the motion about its tether, as being represented by the faster

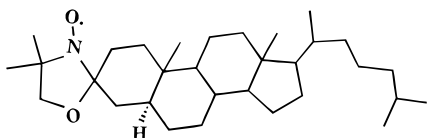


**Figure 1.** Schematic structure of the CSL ( $3\beta$ -doxyl- $5\alpha$ -cholestane) probe.

“probe motion” of the SRLS model. Then the overall backbone reorientation of the polymer, as well as that of nearby polymer molecules, which define the local environment of the probe, becomes the slower relaxing “cage”. The alignment of these LC polymer molecules, which can be macroscopic in the nematic phase, is (weakly) transmitted to the end-chain label, and it is represented by the orienting potential between the probe and the cage in the SRLS model. It is in this spirit that we apply the SRLS model to the analysis of our 2D-FT-ESR spectra, and we demonstrate the greatly improved fits to experiment.

We give details of the preparation of materials and the experimental procedures in section 2. The results and analysis including the NLLS fits to the SRLS model for the 2D-FT-ESR are presented in section 3. Discussion and conclusions appear in sections 4 and 5, respectively.

## 2. Experimental Methods

**2.1. Materials and Characterization.** The LC polymeric samples for 1D and 2D ESR measurements are the same semirigid main chain liquid crystalline poly(ether)s DHMS-7,9 (based on 4,4'-dihydroxy- $\alpha$ -methylstilbene and mixed aliphatic linking groups of 7 and 9 carbons in length) used in the studies reported in the accompanying papers.<sup>8,34</sup> The raw materials (labeled with 3-carboxy-Proxyl free radical and unlabeled) were synthesized and provided by Dr. Elizabeth Hall of the Department of Materials Science and Engineering at Cornell University. The synthesis procedures were described in ref 34. The spin probe CSL ( $3\beta$ -doxyl- $5\alpha$ -cholestane) (cf. Figure 1) was purchased from SIGMA Chemical Co. and used without further purification.

Due to the high spin concentration in raw labeled DHMS-7,9 materials, they need to be diluted by unlabeled DHMS-7,9 to obtain the appropriate spin concentration for ESR studies (cf. ref 34). The procedure is the same for samples with spin probes and spin labels. First, we dissolved CSL spin probe (or labeled DHMS-7,9) in chloroform; then we completely mixed it with a chloroform solution of unlabeled DHMS-7,9. The materials were dried overnight in a vacuum chamber. The samples for the CW-ESR experiment were put into a 1.7 mm i.d. glass tube (3 mm o.d.), further degassed on a vacuum line for several hours, and then sealed after filling with high-purity nitrogen gas. The samples for the 2D-ESR experiment were prepared in a glovebag filled with high-purity nitrogen gas. The dried materials were put into a 2.1 mm i.d. glass tube (2.5 mm o.d.) and sealed by epoxy. After being sealed, both samples were heated up to their isotropic phase and quenched at liquid nitrogen to form tightly packed samples. The spin concentration in these samples was approximately 2–4 mmol (by assuming the density of DHMS-7,9 melt to be 1 g/cm<sup>3</sup>).

The molecular weights of the raw materials were determined by gel permeation chromatography (GPC). The thermal transition temperatures of the raw materials were measured by differential scanning calorimeter (DSC) (cf. section 3.3 of ref 34). These results are listed in Table 1, where  $M_w$  ( $M_n$ ) are the weight (number) average molecular weights,  $T_m$  is the melting transition temperature, and  $T_{ni}$  is the transition temperature from the nematic to the isotropic phase.

**TABLE 1: Molecular Weights and Transition Temperatures of DHMS-7,9 Samples for CW and 2D-FT-ESR Studies**

	species	$M_w$	$M_n$	$T_m$ (°C)	$T_{ni}$ (°C)
samples for 1D experiments	labeled	3300	2700	87	125
	unlabeled <sup>a</sup>	3000	2400	86	123
samples for 2D experiments	labeled	4000	3000	92	118
	unlabeled	4600	3200	90	160

<sup>a</sup> The same unlabeled DHMS-7,9 was used for dilution of labeled DHMS-7,9 and for dissolving the CSL spin probe.

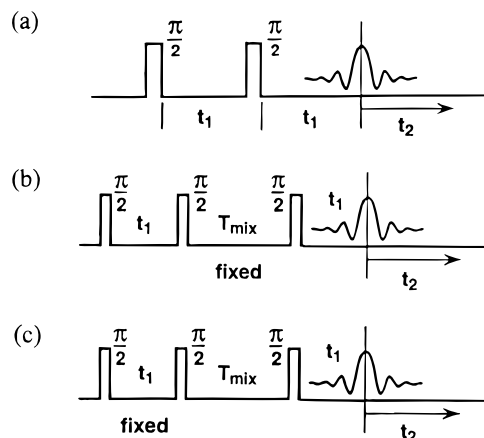


**Figure 2.** 2D-FT-ESR pulse sequences for echo signals: (a) SECSY,  $t_1$  is stepped; (b) ELDOR,  $t_1$  is stepped; (c) stimulated SECSY,  $T_{mix}$  is stepped.

**2.2. CW-ESR Measurements.** All CW-ESR measurements were performed on a Varian Associates, Inc. (Palo Alto, CA) E-12 spectrometer. The spectra were taken in the first-derivative mode, at a constant microwave power without saturation (6.3 mW), during a data acquisition time of 2 min with a 0.128 s time constant. The ESR spectra had 100 G sweep widths. The field modulation frequency was 100 kHz, and its amplitude was chosen in a range of 0.16–1 G to maximize the signal without distorting the spectra. Spectra were digitized to 1024 points and were collected on a 386 PC interfaced to a HP-3457A multimeter. A Varian V6040 variable temperature controller was used to control sample temperature with nitrogen gas. The reported temperature was the temperature at the center of the cavity after calibration. The variation of the temperature over the sample dimension was less than  $\pm 2$  °C.

**2.3. 2D-FT-ESR Measurements.** The 2D-FT-ESR spectrometer has been described elsewhere.<sup>12,14,16</sup> Two basic types of 2D-FT-ESR experiments were performed in our study. The first is the two-pulse experiment of SECSY (spin–echo correlated spectroscopy) ESR, and the second type consists of the three-pulse experiments of 2D-ELDOR (electron–electron double resonance) and stimulated SECSY. SECSY ESR has the advantage of spin–echo spectroscopy by providing the homogeneous line widths (hence the  $T_2$  values) across the inhomogeneously broadened ESR spectrum from which to infer motional dynamics. We were able to detect the echo signal in our LC polymer samples, whereas the FID signal was unavailable due to its very fast decay, (i.e.,  $T_2^* \approx 9$  ns was less than the dead time,  $t_d$ ).

The pulse sequences for the various 2D-FT-ESR experiments (SECSY, ELDOR, stimulated SECSY) are shown in Figure 2. The pulse widths were 5 ns for  $\pi/2$  pulses. The evolution period,  $t_1$ , was sampled with 128 steps of 3 ns size (4.5 ns step size for spectra taken at 24, –47, –107 °C) with an initial  $t_1$  of 50 ns for the SECSY and ELDOR experiments. In stimulated SECSY experiments, the  $t_1$  value of 50 ns was fixed and the  $T_{mix}$  was sampled with 128 steps, and an initial  $T_{mix}$  of 75 ns.

**TABLE 2: NLLS Fit Results from Spin-Labeled DHMS-7,9<sup>a</sup>**

$T$ (°C)	$\Delta$ (G)	$R_{\perp}$ ( $10^7$ s <sup>-1</sup> )	$R_{\parallel}$ ( $10^8$ s <sup>-1</sup> )	$\epsilon_{20}$	$\bar{R}$ ( $10^7$ s <sup>-1</sup> )	$N$	$S$	model
123	1.08	33	16	0	56	5.0	0	isotropic
117	0.97	18.7	11.3	0	34	6.0	0	isotropic
112	0.59	9.6	11.2	0.59	22	12	0.123	aligned
106	0.63	10.9	8.3	0.79	22	7.7	0.172	aligned
102	0.58	10.3	7.4	0.86	20	7.2	0.189	aligned
95	0.67	7.3	6.5	0.51	15	8.9	0.107	momd
91	0.70	7.2	6.4	0.56	15	8.8	0.119	momd
87	0.75	6.6	5.6	0.60	14	8.4	0.129	momd
80	0.66	5.9	4.0	0.60	11	6.7	0.128	momd
68	0.65	4.5	2.6	0.57	8.0	5.9	0.123	momd
58	0.74	3.2	1.8	0	5.7	5.8	0	amor
48	0.78	2.7	1.2	0	4.5	4.6	0	amor
38	1.1	2.3	0.88	0	3.6	3.8	0	amor
29	1.1	2.1	0.56	0	2.9	2.7	0	amor
20	2.1	1.8	0.43	0	2.4	2.4	0	amor

<sup>a</sup> The average percent errors of the NLLS parameters are  $\epsilon_{\Delta} = 4.7$ ,  $\epsilon_{R_{\perp}} = 4.5$ ,  $\epsilon_{R_{\parallel}} = 7.8$ ,  $\epsilon_{\epsilon_{20}} = 3.0$  for  $T > 100$  °C and  $\epsilon_{\Delta} = 10$ ,  $\epsilon_{R_{\perp}} = 6.3$ ,  $\epsilon_{R_{\parallel}} = 12$ ,  $\epsilon_{\epsilon_{20}} = 9$  for  $T < 100$  °C. They were determined from the NLLS fitting procedure as described elsewhere.<sup>8,26</sup>

The step size chosen varied from 30 to 400 ns for stimulated SECSY depending on the decay rate of the signal at each temperature.

The echo signal was collected as a function of  $t_2$  for a total of 256 complex points with a step size of 1 ns (obtained by interleaving<sup>14</sup>) starting at the maximum of echo signal. At each  $t_1$  value (or each  $T_{\text{mix}}$  value for stimulated SECSY), the signal was averaged hundreds to thousands of times for each of the 32 phase cycles steps.<sup>35</sup> A complete 2D experiment took about 20 min to several hours, depending on the repetition rate and the number of averages.

The 2D-FT-ESR experiments (SECSY, ELDOR, stimulated SECSY) were carried out first at room temperature (RT) (24 °C) and then at lower temperatures (−47 and −107 °C). Later we studied the polymer at temperatures above RT (58, 73, 85 °C), up to its nematic phase (100, 111 °C). A series of mixing times,  $T_{\text{mix}}$ , were used for the ELDOR experiments to construct a virtual three-dimensional (3D) data set at each temperature.

The signals were doubly Fourier transformed and utilized for magnitude spectra. No filtering or coverage correction was needed.<sup>24</sup> By linear combination of a dual quadrature signal, we can construct two kinds of signals. The first one is an FID-like signal, because it is not refocused (it is called an  $S_{c+}$  signal). The second one is echo-like, because it is refocused by the pulse sequence (it is an  $S_{c-}$  signal).<sup>25</sup> The  $S_{c-}$  2D spectra are substantially sharper due to the cancellation of the inhomogeneous broadening along the  $t_1$  axis, whereas the  $S_{c+}$  signal typically decayed within the  $t_1$  dead time. Thus just the  $S_{c-}$  signal could be studied.

A Bruker ER 4111 VT variable temperature unit was used to control the sample temperature, which could be varied with cold nitrogen gas. The reported temperature was the temperature at the center of the cavity after calibration. The magnetic field was stabilized at 3355.00 G using a standard field frequency lock (Varian Associates, Palo Alto, CA), with the microwave frequency locked at 9.445730 GHz.

### 3. Results

**3.1. CW-ESR Study.** (a) *End-Labeled Polymer.* These experiments on the end-labeled polymer covered the temperature range from 20 to 123 °C, corresponding to motional states from the near rigid limit to the motional narrowing regime. At

temperatures below 95 °C, no orientation dependent spectra were observed (cf. ref 8). When the sample was heated to temperatures above 98 °C in the magnet, the observed ESR spectra, characterized by the hyperfine splittings (hfs), showed significant macroscopic alignment occurring during the first half hour. An orientation dependent study confirmed that the spin labels possess macroscopic orientational ordering. This result was consistent with what we observed on samples of low MWs during the DID-ESR measurements.<sup>34</sup> The hfs increased as the temperature increased, indicating a reduced ordering. Above 115 °C, the spectra became independent of orientation with respect to the ESR magnetic field, and the hfs was shown to be independent of temperature and greater than that for the macroscopically aligned spectra, indicating that the sample had entered the isotropic phase from the nematic phase.

We started the analysis with the spectra in the nematic phase, in order to take advantage of the macroscopic alignment we obtained for this phase, leading to spectra that have enhanced resolution. This also meant that we could utilize the basic model of reorientation in a macroscopic aligning potential.<sup>27–30</sup> The MOMD model and the “amorphous” model (corresponding to neither macroscopic nor microscopic order) were clearly inappropriate.

We used the same magnetic parameters (in the y-ordering permutation) that were obtained from the rigid limit ESR spectrum at 250 GHz and utilized in ref 8 (cf. Table 1 of ref 8). The four coordinate systems utilized in the simulation were described in detail in ref 8. All spectra were taken at the orientation in which the nematic director coincided with the external magnetic field (i.e.,  $\psi = 0$ ). In our simulation, we found that the case where “diffusion tilt” Euler angle  $\beta = 0^\circ$  produced spectra with no noticeable difference from the case of  $\beta = 10^\circ$ , which was the value found in ref 8. This was true for spectra computed for all temperatures and for the ESR spectra from the CSL spin probe as well. Therefore, we let  $\beta = 0^\circ$  throughout all simulations reported in this section, since the symmetry retained significantly reduces the computation time. The parameters determined by the NLLS fit included the rotational diffusion coefficients,  $R_{\parallel}$  and  $R_{\perp}$  (which relate to molecular motions about the directions parallel and perpendicular to the axis coinciding with the polymer molecular backbone), the Gaussian inhomogeneous broadening,  $\Delta$ , and the potential parameters (cf. ref 8). We also report in Table 2, the geometric average rotational diffusion coefficient,  $\bar{R}$ , the

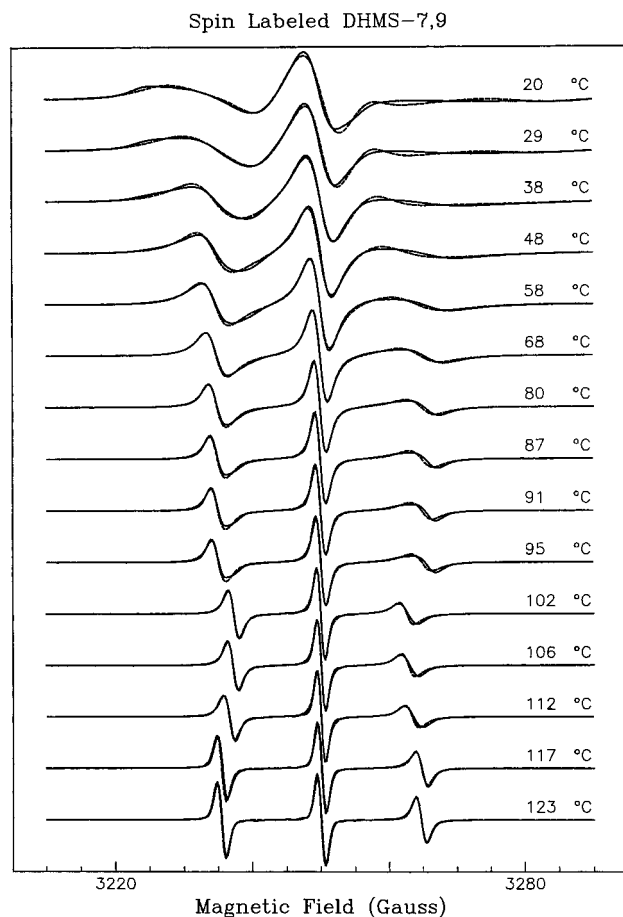


**Figure 3.** Experimental (solid line) and simulated (dashed line) ESR spectra from spin-labeled DHMS-7,9 at various temperatures. Their fitting parameters are listed in Table 2.

rotational anisotropy,  $N$ , and the order parameter,  $S$ , given by

$$\bar{R} = (R_{\perp}^2 R_{\parallel})^{1/3} \quad (1)$$

$$N = R_{\parallel}/R_{\perp} \quad (2)$$

$$S_{2,k} \equiv \langle D_{0k}^2(\Omega) \rangle = \int d\Omega D_{0k}^2(\Omega) \exp\left[-\frac{V(\Omega)}{kT}\right] / \int d\Omega \exp\left[-\frac{V(\Omega)}{kT}\right] \quad (3)$$

$$S \equiv S_{2,0} = \langle D_{00}^2(\Omega) \rangle = \langle (3 \cos^2 \theta - 1)/2 \rangle \quad (4)$$

where  $V(\Omega)$  is the orientational potential function, and just the first term,  $\epsilon_{20}$  in its generalized spherical harmonic expansion (cf. ref 8, eq 1) was sufficient because of the rather low ordering for this case.<sup>36</sup> The experimental and simulated spectra are shown in Figure 3. One notable observation was that within the nematic phase,  $\bar{R}$  was almost independent of temperature, whereas  $S$  was inversely correlated with temperature.

The next set of spectra we fit were those in the isotropic phase, where there is no preferential molecular orientation, (i.e.  $V(\Omega) = 0$ ). In this phase,  $\bar{R}$  was found to increase significantly with increasing temperature.

The spectra below the melting point had no indication of orientation dependent behavior, showing that there was no macroscopic alignment in the solid state. Both the MOMD and amorphous models were initially utilized to study the microscopic dynamics of any local domains. We found that at higher temperatures where the rotational diffusion coefficients were sufficiently large ( $\bar{R} > 6 \times 10^7 \text{ s}^{-1}$ ), i.e.  $T > 65 \text{ }^\circ\text{C}$ , the MOMD

model provided a much better fit to the experimental spectra than the amorphous model. It significantly reduced the deviation between the calculated and experimental data (up to 25%). This shows that the spin labels attached to the polymer chain possess weak local ordering in the solid state, and the effect of ordering upon the ESR spectra is significant when the molecular motion is in the slow motion regime. Note that for motions slow enough that rigid limit ESR spectra are obtained, the MOMD model yields the usual powder spectrum, so in this motional regime it is impossible to distinguish a MOMD model from an amorphous one. This ordering is apparently due to crystallization during the sample preparation process (note that the sample was melted into the isotropic phase and then rapidly cooled down to liquid nitrogen temperature).

When  $\bar{R}$  decreases to less than  $6 \times 10^7 \text{ s}^{-1}$  (i.e.  $T < 65 \text{ }^\circ\text{C}$ ), the MOMD model did not provide a better fit than the amorphous model. We found that at this motional regime the spectra were more sensitive to  $R_{\perp}$  than to either  $R_{\parallel}$  or  $\epsilon_{20}$ , and the fit to the experimental data was not as satisfactory as at the higher temperatures. It is possible that structural parameters such as the three Euler angles specifying the transform between the diffusion frame and the magnetic frame become important when the molecular motion is slow. However, our initial attempts to determine their values from a NLLS fit became very time-consuming and proved unsuccessful because of the excessive number of parameters to be fit to spectra of limited resolution. Therefore, we utilized the amorphous model to simulate these slow motional spectra and kept zero values for the Euler angles for simplicity.

When studying the results of the NLLS fits listed in Table 2, we noticed that the spectrum obtained just above the melting point (i.e.  $T = 102 \text{ }^\circ\text{C}$ ) showed the highest macroscopic ordering amongst all the spectra, including those in the solid. This would seem to imply that macroscopic alignment improves the local ordering within domains. However, the fitting of the disordered solid spectra to the MOMD model leads to greater uncertainty in  $\epsilon_{20}$  compared to that for the better resolved aligned spectra. On the other hand, the detailed analysis of Budil et al.<sup>26</sup> showed that if an imperfect model is used to fit experimental data, which is frequently the case, then the MOMD fit to the basic model that we use seems to return the more reliable values for the parameters, at least in the cases studied. This most probably is because it does include the full range of director orientations, unlike the aligned spectra, for which only the  $\Psi = 0$  orientation is observed. Also, we note that in contrast to its constant behavior in the nematic phase,  $\bar{R}$  increases rapidly after entering the isotropic phase. This "nematic plateau" implies a zero activation energy for  $\bar{R}$  in this phase, which is very similar to observations on the translational diffusion coefficient in this phase, in a temperature dependent study by the FRES (forward recoil spectroscopy) technique on the same model LC polymer system,<sup>37</sup> suggesting some correlation between microscopic rotational diffusion and the macroscopic translational diffusion in this phase.

We show in Figure 4 a plot of  $\log \bar{R}$  as a function of the inverse of temperature,  $1/T$ , leading to the activation energy,  $E_{\text{label}} = (1.16 \pm 0.07) \times 10^4 \text{ J/mol}$ .

(b) *CSL Solute.* CSL has a cigar-like shape, and when it is dissolved into a polymer, it is expected to reveal ordering and dynamic information about its neighboring polymer molecules. The CSL spin probe has been widely used in previous ESR studies, and its magnetic parameters have been determined in various environments.<sup>9,30,38-42</sup> We adapted its  $\mathbf{g}$  and  $\mathbf{A}$  tensor values from those obtained at 250 GHz, but in toluene solvent,<sup>42</sup> with a fine adjustment obtained by fitting a rigid limit X-band

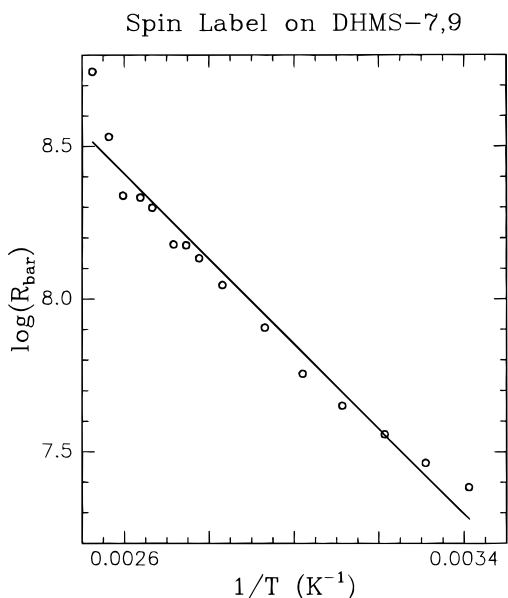


**Figure 4.** Plot of  $\log \bar{R}$  as a function of the inverse of temperature,  $1/T$ , for a spin label on the end of a polymer chain. The overall activation energy,  $E_{\text{label}}$ , is  $(1.16 \pm 0.07) \times 10^4$  J/mol from a linear fit.

**TABLE 3: Magnetic Parameters of CSL in DHMS-7,9**

	<i>xx</i>	<i>yy</i>	<i>zz</i>
<i>g</i>	$2.0084 \pm 0.0003$	$2.0060 \pm 0.0003$	$2.0022 \pm 0.0003$
<i>A</i> (G)	$6.47 \pm 0.5$	$4.50 \pm 0.5$	$32.52 \pm 0.4$

CW spectrum for CSL in DHMS-7,9. We list these *g* and *A* tensors of CSL in Table 3.

Similar to what we observed from spin-labeled DHMS-7,9, we found that the ESR spectra from the CSL probe were orientation dependent in the nematic phase and orientation independent in the isotropic and solid phases. Using the same procedure for fitting the spin label ESR spectra, we performed NLLS fits to these spin probe ESR spectra from the isotropic phase to the solid phase. The isotropic and macroscopically aligned models were utilized to describe the CSL molecular motions in the isotropic and nematic phases, respectively, as we did for spin-labeled DHMS-7,9. We found that the CSL spin probe has a larger rotational anisotropy and slower rotational diffusion coefficients ( $\bar{R}$  and  $R_{\perp}$ ) than the spin label at the end of the polymer chain and a larger macroscopic ordering (*S*) in the nematic phase. Since the spin probes were dissolved in polymer molecules, and thus their dynamics reflected the overall polymer backbone motion, this result suggests that the polymer end has much greater rotational mobility than the polymer backbone. The “nematic plateau” was again observed in this spin probe experiment; that is, the average rotational coefficient  $\bar{R}$  is independent of the temperature within the nematic phase.

Below the melting point, the rotational diffusion of the CSL probe is slow enough that the MOMD model no longer shows any significant effect on the ESR spectra, compared to the amorphous model, so the latter (simpler) model was applied for these spectra. Both  $\bar{R}$  and the rotational anisotropy, *N*, were found to increase when the temperature increases. These results are summarized in Table 4. The experimental and simulated spectra are plotted in Figure 5.

The activation energy for CSL,  $E_{\text{probe}}$ , obtained from a linear fit to the plot of  $\log \bar{R}$  as a function of  $1/T$ , was found to be  $(1.64 \pm 0.03) \times 10^4$  J/mol (cf. Figure 6), about 40% greater than that for the spin label attached to the end of the polymer molecule. To compare the ordering of the end-labeled DHMS-

7,9 and the CSL spin probe, we plot their potential coefficients,  $\epsilon_{20}$ , as a function of temperature over the melt phases in Figure 7. It is found that the CSL probe possesses higher ordering than the polymer end-label in the nematic, as we would expect, since it is expected to reflect the overall dynamic structure of the polymer molecules.

**3.2. 2D-FT-ESR Study.** The 2D-FT-ESR experiments were performed at eight temperatures. At each temperature, we measured stimulated SECSY, SECSY, and 2D-ELDOR. Five to nine values of mixing time,  $T_{\text{mix}}$ , were chosen ranging from 0 to 2  $\mu\text{s}$  at the highest temperatures and 0 to 50  $\mu\text{s}$  at the lowest temperatures for the ELDOR experiments to construct a virtual 3D data set. In this context we note that a SECSY experiment is the equivalent<sup>25</sup> of a 2D-ELDOR experiment with  $T_{\text{mix}} = 0$ . In Figure 8 we include ELDOR spectra from each temperature at a mixing time of 1  $\mu\text{s}$ . These eight spectra show the thermal behavior of the LC polymer observed by 2D-ELDOR.

We noticed that below the solid to nematic phase transition temperature,  $T_m$ ,<sup>43</sup> the 2D-ELDOR spectra did not show any significant cross-peaks, which would develop from cross-relaxation mechanisms.<sup>12–14,19</sup> These include the intramolecular electron–nuclear dipolar (END) interaction, which leads to nuclear flip rates,  $W_n$ , and Heisenberg spin exchange (HE) rates,  $\omega_{\text{HE}}$ . One can distinguish the two mechanisms because the  $W_n$  contributes primarily to the  $\Delta M_1 = \pm 1$  (single-quantum) cross-peaks, whereas  $\omega_{\text{HE}}$  contributes equally to the  $\Delta M_1 = \pm 1$  and  $\pm 2$  cross-peaks. Our experiment showed a virtual absence of cross peaks at all mixing times below  $T_m$ , indicating that both the HE and END contributions were very weak in the solid phase.

Based on our previous ESR work,<sup>8,34</sup> as well as the sample studied in section 3.1, it is clear that the DHMS-7,9 sample used in this 2D-FT-ESR study would be macroscopically aligned by the X-band ESR magnetic field in the nematic phase. This was indeed the case, so that the 2D spectra became significantly sharper after the sample temperature was brought above 94 °C for more than half an hour. The macroscopically aligned 2D spectra obtained in the nematic phase yielded enhanced resolution compared to the lower temperatures, in addition to the increased molecular motion. The hyperfine splitting between the two peaks in the SECSY spectrum (cf. Figure 9a) was consistent with what we observed from the macroscopically aligned CW-ESR spectra. The single-quantum ( $\Delta M_1 = \pm 1$ ) cross-peak in the 2D-ELDOR spectra grew with mixing time, and reached a maximum for  $T_{\text{mix}} = 600$  ns at 111 °C (cf. Figure 9). However, even with the enhanced resolution in the nematic phase, no double-quantum ( $\Delta M_1 = \pm 2$ ) cross-peak was observed. Therefore, we concluded that in this spin-labeled system the spin concentration is too low to show an appreciable HE effect.

We performed NLLS fits to these 2D-FT-ESR spectra to extract the dynamic and ordering information. At present, we can fit SECSY (corresponding to 2D-ELDOR where  $T_{\text{mix}} = 0$ ) and several 2D-ELDOR spectra simultaneously, i.e., a virtually 3D NLLS fit. We first fit experimental data at the highest temperature studied (111 °C) corresponding to the nematic phase. Whereas the standard model of rotational diffusion in a macroscopic aligning potential led to a very good fit to the CW-ESR spectra, as we showed in the preceding section, the 2D spectra with effectively two additional spectral dimensions reveal more detailed dynamic information that could not be fit with such a simple model for the molecular dynamics. This standard model did not fit the 2D data in key features, particularly in the magnitudes of the single-quantum cross-peaks relative to the auto peaks (cf. Figure 9).

TABLE 4: NLLS Fit Results from a CSL Spin Probe in DHMS-7,9<sup>a</sup>

$T$ (°C)	$\Delta$ (G)	$R_{\perp}$ ( $10^7$ s <sup>-1</sup> )	$R_{\parallel}$ ( $10^8$ s <sup>-1</sup> )	$\epsilon_{20}$	$\bar{R}$ ( $10^7$ s <sup>-1</sup> )	N	S	model
139	1.8	5.7	27	0	21	47	0	isotropic
130	1.8	4.5	16	0	15	36	0	isotropic
127	1.7	4.1	13	0	13.	32	0	isotropic
122	1.6	3.1	16	0.18	12	53	0.036	aligned
117	1.4	3.0	13	1.36	10	44	0.30	aligned
112	1.5	3.1	9.5	1.76	9.8	30	0.39	aligned
106	1.6	3.0	12	2.00	10	40	0.44	aligned
93	1.2	1.5	3.0	0	4.0	20	0	amor
82	1.4	1.2	2.1	0	3.1	18	0	amor
70	1.6	0.98	1.2	0	2.3	12	0	amor
59	2.1	0.75	0.71	0	1.6	9.5	0	amor
50	3.0	0.47	0.44	0	0.90	9.3	0	amor
41	3.8	0.28	0.26	0	0.59	9.0	0	amor
34	4.3	0.23	0.19	0	0.46	8.0	0	amor
29	4.6	0.17	0.14	0	0.34	8.0	0	amor

<sup>a</sup> The average percent errors of the NLLS parameters are  $\epsilon_{\Delta} = 6.2$ ,  $\epsilon_{R_{\perp}} = 6$ ,  $\epsilon_{R_{\parallel}} = 12$ ,  $\epsilon_{\epsilon_{20}} = 3.5$  for  $T > 100$  °C and  $\epsilon_{\Delta} = 11$ ,  $\epsilon_{R_{\perp}} = 8$ ,  $\epsilon_{R_{\parallel}} = 15$  for  $T < 100$  °C. They were determined from the NLLS fitting procedure as described elsewhere.<sup>8,26</sup>

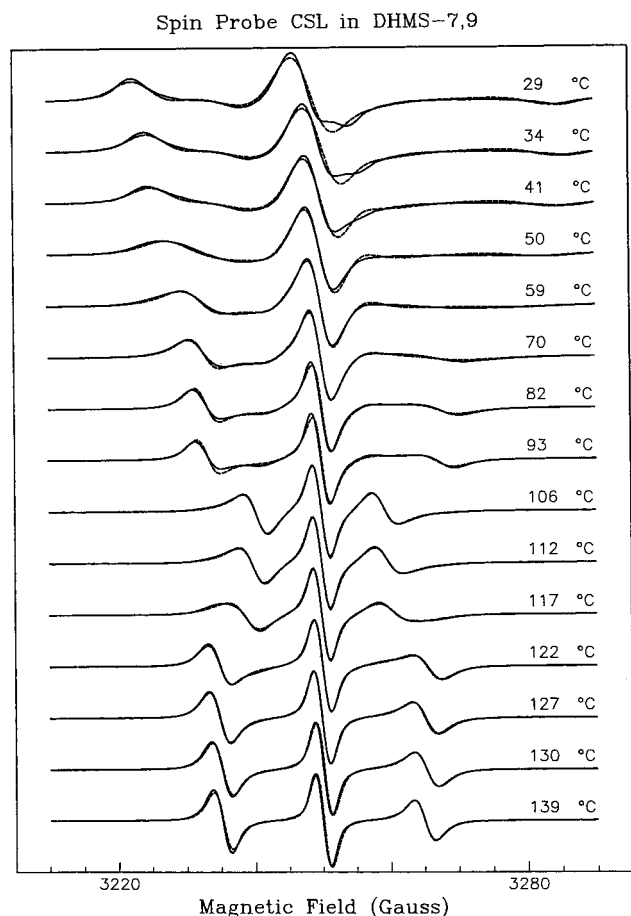


Figure 5. Experimental (solid line) and simulated (dashed line) ESR spectra from spin probe CSL in DHMS-7,9 at various temperatures. Their fitting parameters are listed in Table 4.

To try to improve agreement with experiment, we used the Polimeno–Freed model of SRLS appropriate for slow motional ESR simulations (cf. section 1 and refs 31, 33). As we have employed it in our NLLS fitting to the sets of 2D-ELDOR spectra, we describe the local motion of the end-label by an effective axial rotational diffusion tensor specified by  $R_{\perp}$  and  $R_{\parallel}$ . The backbone structure of the polymer to which the nitroxide is attached as well as any contributions to the “cage” experienced by the end-label from adjacent molecules is allowed to relax with a diffusion coefficient,  $R^c$ . We assume, for the sake of simplicity, that the cage (i.e., the set of relevant polymer molecules) experiences a cylindrically symmetric macroscopic

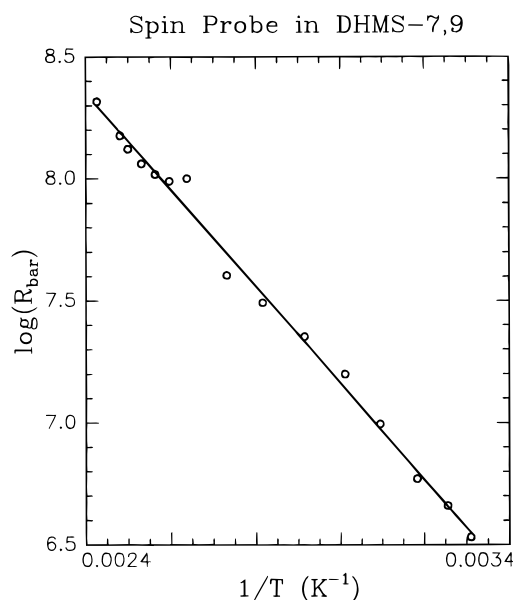
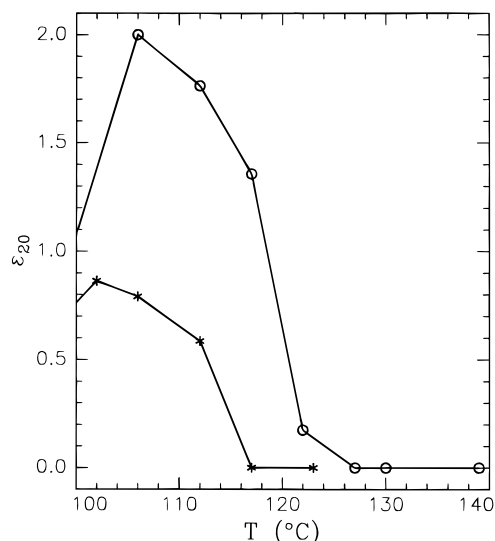


Figure 6. Plot of  $\log \bar{R}$  as a function of the inverse of temperature,  $1/T$ , for spin probe CSL dissolved in LC polymer DHMS-7,9. The overall activation energy,  $E_{\text{probe}}$ , is  $(1.64 \pm 0.03) \times 10^4$  J/mol from a linear fit.

orienting potential in the nematic phase and that furthermore the end-label prefers to align with its magnetic  $y$ -axis parallel to the principal axis of cage alignment, which is analogous to the simple  $y$ -axis alignment we used in simulating the CW-ESR spectra (cf. section 3.1 and ref 8). Given these symmetries, we note that  $R^c$  more precisely equals  $R_{\perp}^c$ , the perpendicular component of a “cage” diffusion tensor, and  $R_{\parallel}^c$ , the parallel component, has no effect on the spectrum. Thus in our model the polymer backbone is macroscopically aligned with its nematic director parallel to the magnetic field, while the ordering of the end-labels is due to its coupling to the “cage”. Also, it is sufficient to represent the “cage” alignment by the potential parameter  $b_{2,0}$  according to  $V(\Omega^c)/kT = -b_{2,0}D_{0,0}^2(\Omega^c)$ , where  $D_{M,K}^L(\Omega^c)$  is a generalized spherical harmonic, and the alignment of the end-label relative to this “cage” is specified by the two orienting potential coefficients,  $c_{20}$  and  $c_{22}$ , as described further in the next section, (cf. eq 5). (Although the case that has a mean field potential for the label instead of for the cage leads to a comparable quality of fit, the calculated spectra did not produce as good a relative intensity of the peaks as the case we chose to use.)



**Figure 7.** Plot of potential coefficient,  $\epsilon_{30}$ , as a function of temperature,  $T$ , for spin label (\*) and spin probe CSL (O) in LC polymer DHMS-7,9.

The spectra obtained in the nematic phase (100, 111 °C) were both NLLS fit by this SRLS model, and we found that it led to a greatly improved quality of fit in comparison with the simple model of macroscopic alignment and Brownian motion. We plot experimental SECSY and ELDOR spectra at 111 °C, and their best fit using both the SRLS and standard models for comparison, as shown in Figure 9.

Below the melting point, the polymer backbone had no macroscopic alignment. However, the crystallization resulting from the isotropic to solid phase (room temperature) transition during the sample preparation is expected to introduce a local ordering of the spin labels, as we observed in the CW-ESR study. Such a case can be well described by the more conventional MOMD model to simplify the spectral analysis. It is equivalent to the limiting case of the SRLS model in which the motion of the cage is too slow to affect the spectrum. (We initially attempted to use the SRLS model to fit the spectra at 85 °C. However, with the largest basis set that our current computing capability can handle, the slowest cage rotational rate ( $5 \times 10^4 \text{ s}^{-1}$ ) is still too fast for optimum fits; in particular, it generates sufficiently large cross-peaks that were not observed from the experimental spectra. This corresponds to a  $\chi^2$  error that is 50% greater than the fits to the spectra in nematic phase.) It is very likely that the virtual absence of any cross-peaks in the solid phase 2D-ELDOR spectra is primarily due to the MOMD broadening. Therefore, the basic MOMD model was used to fit the spectra at the two temperatures 85° and 73 °C, which lie below the melting point.<sup>44</sup> The experimental and simulated spectra of 73 °C are plotted in Figure 10.

We list all the parameters extracted from NLLS fit to these 3D data in Table 5, and we shall compare the 2D-FT-ESR results with those obtained from CW-ESR studies on spin-labeled DHMS-7,9 and CSL dissolved in DHMS-7,9 in the next section.

#### 4. Discussion

The principal result we have obtained is the dramatic difference between the predicted 2D-FT-ESR spectra for the SRLS model (or its limiting MOMD model) and the standard model of Brownian reorientation in an orientational potential. Whereas the latter gives very poor agreement with experiment, the former gives much better, though not perfect, agreement

with experiment. The CW-ESR spectra, on the other hand, are rather well fit by the standard model, and there is no reasonable justification for introducing the extra model parameters, required in the SRLS model, to fit the X-band CW-ESR spectra with their limited resolution to dynamics and their limited information content (i.e., 1D vs effectively 3D spectral degrees of freedom). Nevertheless, the CW-ESR spectra are still useful in monitoring overall trends in the ordering and dynamics.

When we compare the 2D-FT-ESR and CW-ESR results for the end-labeled polymer, we find that the local dynamic parameters  $R_{\perp}$  and  $R_{\parallel}$  are systematically somewhat higher for the CW-ESR fits. More precisely,  $R_{\perp}$  is 2–3 times larger, while  $R_{\parallel}$  is about 20–40% greater. In the slow motional regime, an increase in  $R_{\perp}$  yields greater line broadening.<sup>1,28,29</sup> When SRLS (or MOMD) is present in this regime, there is additional line-broadening, but of an inhomogeneous type. Failure to include this SRLS (or MOMD) model in a fit means that one must compensate by increasing  $R_{\perp}$ . A virtue of the 2D-FT-ESR experiment is that it allows one to distinguish homogeneous and the various types of inhomogeneous broadening, and this is one source of the better spectral resolution to ordering and dynamics compared to CW-ESR.<sup>23–25</sup> Note that the values of  $R_{\perp}$  and  $R_{\parallel}$  obtained for the fit to the 111 °C 2D-FT-ESR spectra using the standard model (cf. caption to Figure 9) are quite close to those obtained using the SRLS model (cf. Table 5). Instead, the additional inhomogeneous broadening appears as a substantial increase in  $\Delta$  (the Gaussian broadening) for the standard model vs SRLS.

These comments are most relevant for a comparison of our results in the nematic phase where SRLS was used for the 2D-FT-ESR analysis and the standard model was used for the CW-ESR. In the solid phase the MOMD model was used for both types of experiments, yet even larger differences in  $R_{\perp}$  were found. Simply stated, the NLLS fitting had to reduce the  $R_{\perp}$  to be consistent with the observed absence of ( $\Delta M_1 = \pm 1$ ) cross-peak development in the 2D-ELDOR experiments in this phase. But this also required a substantially larger  $\Delta$ , the extra inhomogeneous broadening, for these 2D-ELDOR fits. We take these features to imply the use of an imperfect model, viz., MOMD rather than SRLS for the practical reasons outlined in the previous section. Also we have not allowed for any heterogeneities in the polymer, which could lead to a distribution in, for example, cage properties.

We note that the 2D-FT-ESR spectral fitting was not very sensitive to the value of  $R_{\parallel}$ , as is typically the case for slow motional CW-ESR, although both 2D-FT-ESR and CW-ESR yielded an  $N$  on the order of 10.

In ref 8, it was found that the dynamics of the end-label does depend somewhat on the molecular weight of the matrix polymer, and there is some difference between that for the CW experiment ( $M_w = 3000$ ) and that for the 2D-FT-ESR experiments ( $M_w = 4600$ ). This could lead to a moderate increase in  $R_{\perp}$  for the lower molecular weight CW-ESR sample, which is also consistent with our fits. However, it should be appreciated that the structure of the “cage”, within which the end-label engages in its local motions, should be sensitive to the matrix molecular weight. In fact, in ref 8 the matrix MW dependence of  $R_{\perp}$  was interpreted in terms of the free volume available to the end-label. Clearly, it would be interesting to explore in some future study how the dynamic “cage” properties predicted from a SRLS analysis of 2D-ESR experiments depend upon matrix MW.

In the case of the ordering predicted from both experiments, this is easier to compare for the solid phase where the same

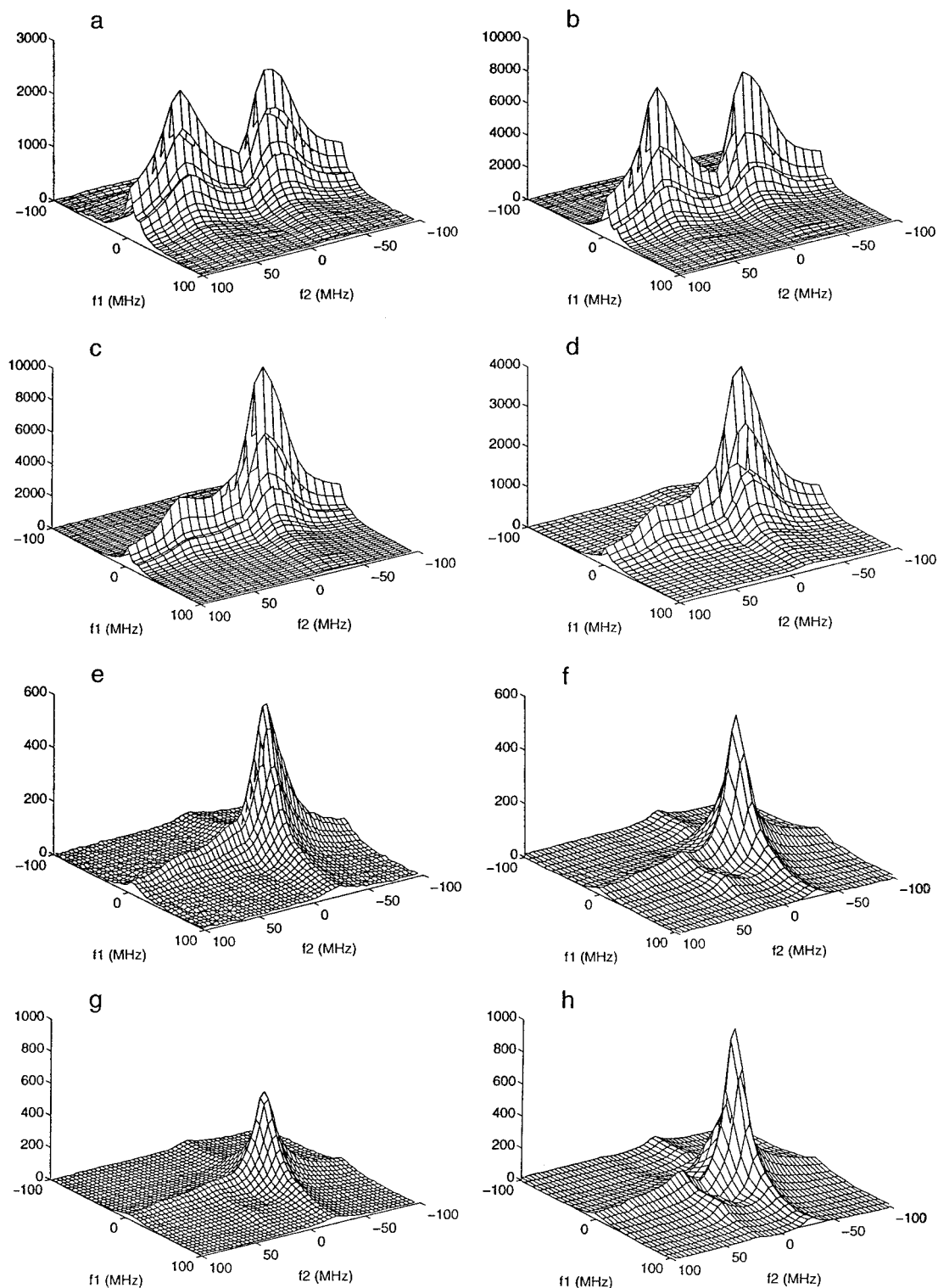


**Figure 8.** 2D-ELDOR spectra (arbitrary magnitudes) at a mixing time  $T_{\text{mix}} = 1 \mu\text{s}$  at various temperatures: (a)  $-107^\circ\text{C}$ ; (b)  $-47^\circ\text{C}$ ; (c)  $24^\circ\text{C}$ ; (d)  $58^\circ\text{C}$ ; (e)  $85^\circ\text{C}$ ; (f)  $94^\circ\text{C}$ ; (g)  $100^\circ\text{C}$ ; (h)  $111^\circ\text{C}$ .

MOMD model was used. Both experiments lead to an order parameter  $S \approx 0.13$ . In the nematic phase, our use of a SRLS model, in which the macroscopic alignment only directly affects the polymer backbones, whereas the end-label experiences the macroscopic alignment indirectly via its coupling to the “cage” formed by the nearby polymers, leads to a less precisely defined macroscopic order parameter. For such cases,<sup>45</sup> it is usually given as  $S_1 \approx S_{\text{overall}}S_{\text{internal}}$  when the two averaging processes are approximately independent, where  $S_{\text{overall}} \approx 0.27$  is derived from the  $b_{2,0}$  values in Table 5, while  $S_{\text{internal}} \approx 0.14$  is from

the  $c_{20}$  and  $c_{22}$  values also in Table 5. (These values are for  $100^\circ\text{C}$ ). Thus we would estimate  $S_1 \approx 0.04$ , which would imply a reduced effective ordering using the fits to the SRLS model. In addition there is a nonaxial order parameter<sup>1</sup>,  $S_{2,\text{internal}} \equiv 2\langle \text{Re} D_{02}^2(\Omega) \rangle \approx 0.29$ .

We now consider in further detail the potential function describing the microscopic alignment of the spin label at the end of the polymer main chain, with respect to the cage axis, i.e., the backbone of the polymer molecule. This potential function may be written as<sup>31</sup>

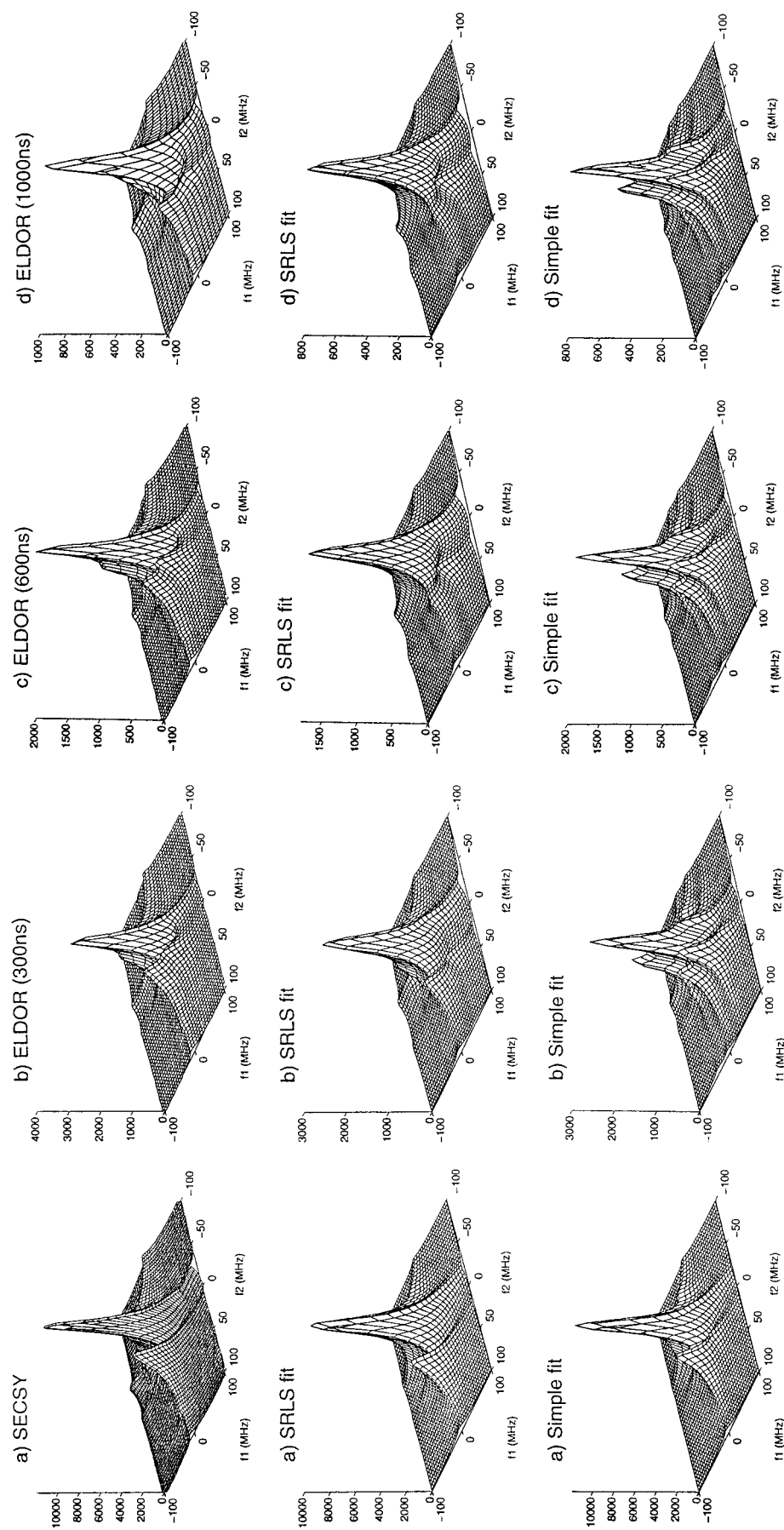


**Figure 9.** 2D-FT ESR spectra (arbitrary magnitudes) at 111 °C, the experimental (top row), simulated by SRLS model (middle row), and simulated by standard Brownian model (bottom row): (a) SECSY ( $T_{\text{mix}} = 0$  ns); (b) ELDOR ( $T_{\text{mix}} = 300$  ns); (c) ELDOR ( $T_{\text{mix}} = 600$  ns); (d) ELDOR ( $T_{\text{mix}} = 1000$  ns). SRLS fitting parameters are listed in Table 5. Fitting parameters for standard Brownian model are  $\Delta = 0.98$  G,  $R_{\perp} = 6.17 \times 10^7$  s $^{-1}$ ,  $R_{\parallel} = 7.34 \times 10^8$  s $^{-1}$ , and  $\epsilon_{20} = 1.42$ .

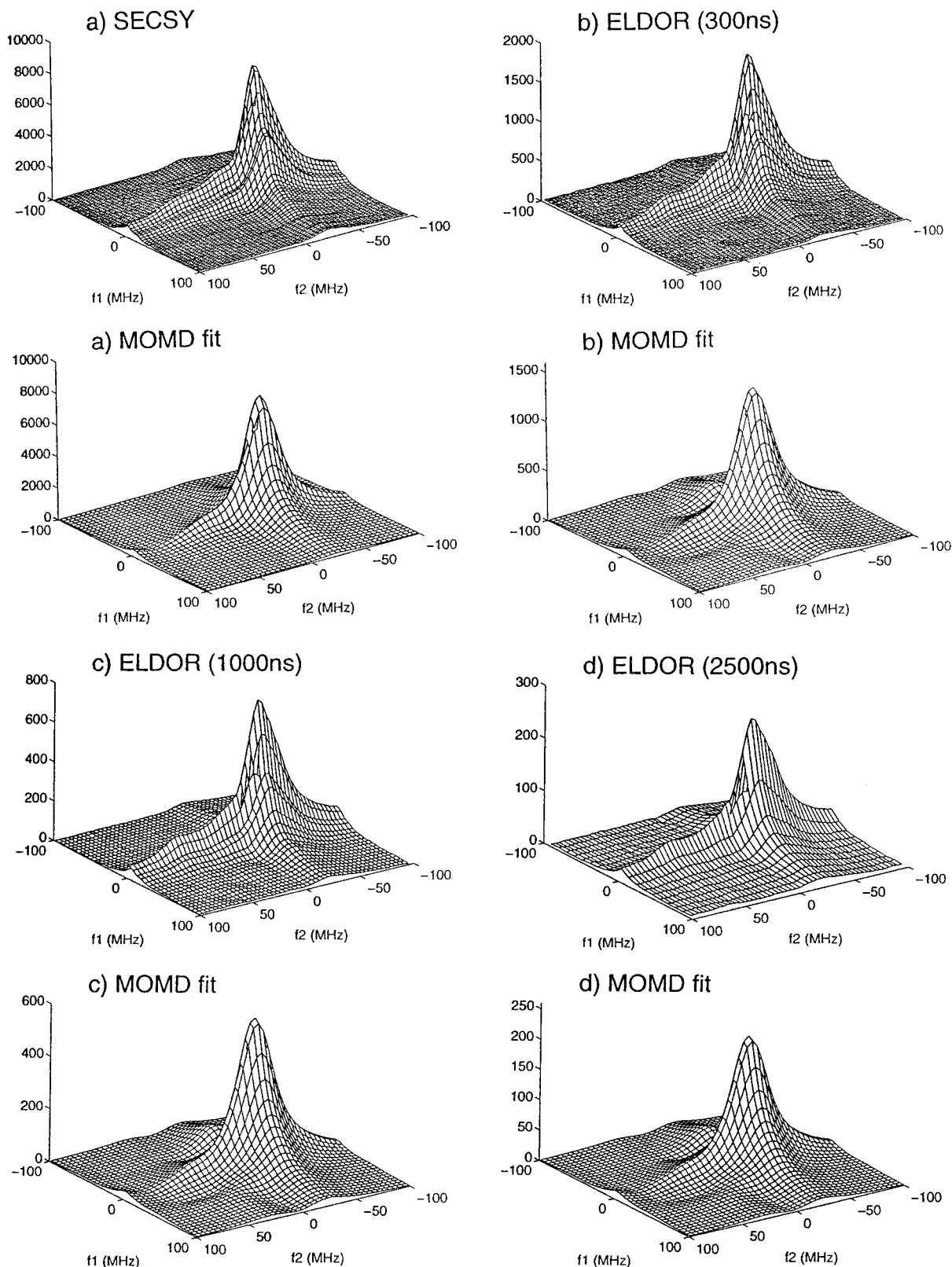


**Figure 10.** 2D-FT ESR spectra (arbitrary magnitude) at 73 °C, the experimental (upper) and simulated by MOMD model: (a) SECSY; (b) ELDOR ( $T_{\text{mix}} = 300$  ns); (c) ELDOR ( $T_{\text{mix}} = 1000$  ns); (d) ELDOR ( $T_{\text{mix}} = 2500$  ns). MOMD fitting parameters are listed in Table 5.

$$u(\theta, \phi) \equiv \frac{V(\Omega)}{kT} = - \sum_{L,M,K} c_{MK}^L D_{MK}^L(\Omega) = - \frac{1}{2} c_{20} (3 \cos^2 \theta - 1) - \sqrt{\frac{3}{2}} c_{22} \sin^2 \theta \cos 2\phi \quad (5)$$

where  $\theta$  and  $\phi$  represent the polar and azimuthal angles of the

polymer main chain  $z_c$  axis, which is taken as the principal axis of the cage in the molecular axis system ( $x'$ ,  $y'$ ,  $z'$ ), which is the principal axis system of alignment of the end-label, and following standard practice, we take it to be collinear with the principal axis system of the diffusion tensor. Since we used  $y'$ -ordering as described in ref 8, the  $z'$ -axis is parallel to the  $y''$ -axis, and  $x''' \parallel |y', z''| \parallel x'$ , where by convention  $x'''$  is defined as parallel to the N–O bond of the free radical, and  $z'''$  is defined

**TABLE 5: NLLS Fit to 2D-FT-ESR from Spin-Labeled DHMS-7,9<sup>a</sup>**

$T$ (°C)	$\Delta$ (G)	$R_{\perp}$ ( $10^7$ s <sup>-1</sup> )	$R_{\parallel}$ ( $10^8$ s <sup>-1</sup> )	$c_{20}$ or $\epsilon_{20}^b$	$c_{22}$ or $\epsilon_{22}^b$	$\bar{R}$ ( $10^7$ s <sup>-1</sup> )	N	S	$R^c$ ( $10^5$ s <sup>-1</sup> )	$b_{20}$	model
111	0.60	5.9	8.5	0.39	0.84	14	14		3.3	1.00	SRLS
100	0.59	4.8	6.7	0.91	1.01	12	14		1.7	1.45	SRLS
85	2.59	2.2	4.0	0.84	1.00	5.8	18	0.126			MOMD
73	2.80	1.5	2.8	0.81	0.90	4.0	18	0.130			MOMD

<sup>a</sup> The average percent errors of the NLLS parameters are  $\epsilon_{\Delta} = 2.4$ ,  $\epsilon_{R_{\perp}} = 4.1$ ,  $\epsilon_{R_{\parallel}} = 5.3$ ,  $\epsilon_{c_{20}} = 3.8$ ,  $\epsilon_{c_{22}} = 4.2$ ,  $\epsilon_{R^c} = 5.6$ , and  $\epsilon_{b_{20}} = 5.4$ . They were determined from the NLLS fitting procedure as described elsewhere.<sup>8,26</sup> <sup>b</sup>  $c_{20}$  and  $c_{22}$  refer to the SRLS model, whereas  $\epsilon_{20}$  and  $\epsilon_{22}$  refer to the MOMD model.

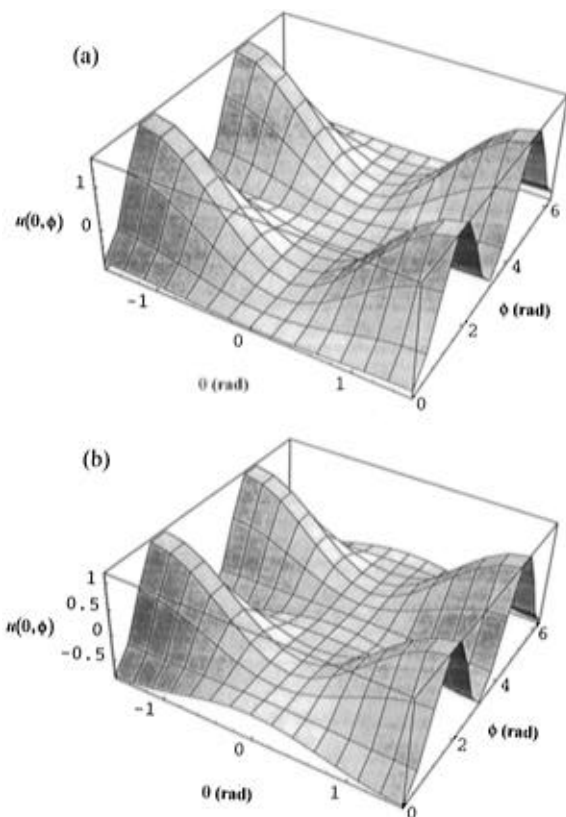


**Figure 11.** SRLS potential functions  $u(\theta, \phi)$  obtained from the best fit values listed in Table 5 and eq 4: (a)  $T = 100$  °C,  $c_{20} = 0.91$ ,  $c_{22} = 1.01$ ; (b)  $T = 111$  °C,  $c_{20} = 0.39$ ,  $c_{22} = 0.84$ .

as parallel to the axis of the N–O  $\pi$  orbital (cf. Figure 1 of ref 8). We plot the potential function defined by eq 5 and the  $c_{20}$ ,  $c_{22}$  results at 100 and 111 °C in Figure 11. The simplicity and symmetry of eq 5 dictates that the potential extrema must always lie along one of these principal axes. This corresponds to the minimum at  $\theta = 0$  in Figure 11; that is,  $u(\theta, \phi)$  is a minimum for  $y'''|z_c$  for both temperatures, making it a preferred orientation, as we expected. However, at 111 °C the minimum at  $\theta = \pi/2$ ,  $\phi = 0$  or  $\pi$  lies slightly lower. It corresponds to the  $z'''$ -axis being aligned along  $z_c$ .

When we compare the  $R_{\perp}$  for the end-label with that of the CSL probe, using the CW-ESR results for comparison, we find that the reorientation of CSL is significantly slower (about 5 times slower). This is as expected since the nitroxide moiety of CSL cannot reorient by any internal chain rotations and thus is more sensitive to the polymer backbone rotation. In this comparison we cannot distinguish relative differences due to local motions of the probe vs those of the cage.

We note from the 2D-FT-ESR study that the cage motion is more than 2 orders of magnitude slower than that of the end-label, consistent with our expectations of much slower polymer backbone reorientations than local internal motions. Furthermore, the cage motion has a larger temperature dependence than

the probe motion, implying this motion has a higher activation energy. While the  $R^c$  value of the cage increased by a factor of 2 from 100 to 111 °C, the  $\bar{R}$  value of the spin label increased slightly, by only 24%. We utilized the results from the two temperatures in the nematic phase to obtain a crude estimate of the activation energy of the “cage”, which yielded  $3.2 \times 10^4$  J/mol. The activation energy of the end-label estimated from the 2D data is  $1.0 \times 10^4$  J/mol, very close to its value of  $1.2 \times 10^4$  J/mol obtained from the CW-ESR study and a little smaller than the activation energy estimated for CSL from its CW-ESR study, of  $1.6 \times 10^4$  J/mol. Due to the limited temperature dependent 2D-FT-ESR results in the nematic phase, we were not able to distinguish the “nematic plateau” observed in the 1D-CW-ESR studies. Future 2D-FT-ESR experiments would be helpful to further study this phenomenon.

## 5. Conclusions

1. Both 2D-FT-ESR (SECSY, ELDOR, stimulated SECSY) and CW experiments have been successfully performed to study the rotational molecular dynamics and ordering of the LC polymer system.

2. From a CW-ESR temperature dependent study, we found the spin labels attached to the end of the polymer chain possess greater mobility and reduced order than the CSL spin probe dissolved in the polymer. The former is significantly influenced by the local internal modes of motion of the end-chain, whereas the latter reflects the overall molecular dynamics of neighboring polymer molecules. The overall activation energy for the CSL is greater than that of the end-label.

3. The LC polymer system in our study was found to exhibit microscopic ordering but no macroscopic ordering in its solid phase, but it was macroscopically ordered in the nematic phase by the ESR magnetic field of 3300 G.

4. The average rotational diffusion coefficient of both the spin label and spin probe appeared to be independent of temperature within the nematic phase from the 1D-CW-ESR study. This “nematic plateau” phenomenon was very similar to that observed for the translational diffusion coefficient measured by the FRES technique on the same LC polymer system, indicating there might be some correlation between the microscopic rotational and the macroscopic translational motions.

5. The greatly enhanced resolution in 2D-FT ESR spectra (especially in the 3D format obtained as a function of mixing time,  $T_{\text{mix}}$ ) in combination with nonlinear least squares spectral analysis enables one to extract more detailed information about the molecular reorientational process.

6. Using the slowly relaxing local structure model, we were able to distinguish the local reorientational motion of the end-label from the more slowly relaxing “cage” formed by the polymer molecule to which it is attached as well as by the neighboring polymer molecules.

**Acknowledgment.** We would like to gratefully thank Dr. E. Hall for the supply of the DHMS-7,9 samples, Dr. D. E.

Budil for his help with the spectral simulations, and S. Saxena for the help in carrying out the 2D experiments and improving some 2D figures. This work was supported by the MRL Program of the National Science Foundation under Award No. DMR-9121654 and by NSF Grant No. DMR-9210638 and NIH Grant Nos. GM-25862 and RR07126. The Cornell Theory Center and the Cornell Materials Science Center are also acknowledged.

## References and Notes

- (1) Freed, J. H.; Nayeem, A.; Rananavare, S. B. In *The Molecular Dynamics of Liquid Crystals*; Luckhurst, G. R., Veracini, C. A., Eds.; Kluwer Academic Publishers: Netherlands, 1994; Chapters 12–15, and references therein.
- (2) Shin, Y.-K.; Budil, D. E.; Freed, J. H. *Biophys. J.* **1993**, *65*, 1283.
- (3) Pilar, J.; Labsky, J.; Kalal, J.; Freed, J. H. *J. Phys. Chem.* **1979**, *83*, 1907.
- (4) Shiotani, M.; Sohma, J.; Freed, J. H. *Macromolecules* **1983**, *16*, 1495.
- (5) Müller, K.; Wassmer, K.-H.; Lenz, R. W.; Kothe, G. *J. Polym. Sci., Polym. Lett.* **1983**, *21*, 785.
- (6) Meurisse, P.; Friedrich, C.; Dovlitzky, M.; Lauprêtre, F.; Noël, C.; Monnerie, L. *Macromolecules* **1984**, *17*, 72.
- (7) Ge, M.; Freed, J. H. *Biophys. J.* **1993**, *65*, 2106.
- (8) Xu, D.; Budil, D. E.; Ober, C. K.; Freed, J. H. *J. Phys. Chem.* **1996**, *100*, 15867.
- (9) Kar, L.; Ney-Igner, E.; Freed, J. H. *Biophys. J.* **1985**, *48*, 569.
- (10) Seelig, J. *Q. Rev. Biophys.* **1977**, *10*, 353.
- (11) Gorcester, J.; Freed, J. H. *J. Chem. Phys.* **1986**, *85*, 5375.
- (12) Gorcester, J.; Freed, J. H. *J. Chem. Phys.* **1988**, *88*, 4678.
- (13) Gorcester, J.; Millhauser, G. L.; Freed, J. H. In *Advanced EPR: Applications in Biology and Biochemistry*; Hoff, A. J., Ed.; Elsevier: Amsterdam, 1989; Chapter 5.
- (14) Gorcester, J.; Millhauser, G. L.; Freed, J. H. In *Modern Pulsed and Continuous Wave Electron Spin Resonance*; Kevan, L., Bowman, M. K., Eds.; Wiley: New York, 1990.
- (15) Bowman, M. K. In *Modern Pulsed and Continuous-Wave Electron Spin Resonance*; Kevan, L., Bowman, M. K., Eds.; Wiley: New York, 1990.
- (16) Lee, S.; Patyal, B. R.; Freed, J. H. *J. Chem. Phys.* **1993**, *98* (5), 3665.
- (17) Schweiger, A. In *Modern Pulsed and Continuous-Wave Electron Spin Resonance*; Kevan, L., Bowman, M. K., Eds.; Wiley: New York, 1990.
- (18) A recent example of this type of experiment is given by: Pöpl, A.; Kevan, L.; *J. Phys. Chem.* **1996**, *100*, 3387.
- (19) Gorcester, J.; Rananavare, S. B.; Freed, J. H. *J. Chem. Phys.* **1989**, *90*, 5764.
- (20) Fauth, J.-M.; Kababya, S.; Goldfarb, D. *J. Magn. Reson.* **1991**, *92*, 203.
- (21) Plüschau, M.; Dinse, K.-P. *J. Magn. Reson.* **1994**, *A109*, 181.
- (22) Patyal, B. R.; Crepeau, R. H.; Gamliel, D.; Freed, J. H. *Chem. Phys. Lett.* **1990**, *175*, 445, 453.
- (23) Lee, S.; Patyal, B. R.; Saxena, S.; Crepeau, R. H.; Freed, J. H. *Chem. Phys. Lett.* **1994**, *221*, 397.
- (24) Crepeau, R. H.; Saxena, S.; Lee, S.; Patyal, B. R.; Freed, J. H. *Biophys. J.* **1994**, *66*, 1489.
- (25) Lee, S.; Budil, D. E.; Freed, J. H. *J. Chem. Phys.* **1994**, *101* (7), 5529.
- (26) Budil, D. E.; Lee, S.; Saxena, S.; Freed, J. H. *J. Magn. Reson.* **1996**, *A120*, 155.
- (27) Ge, M.; Budil, D. E.; Freed, J. H. *Biophys. J.* **1994**, *66*, 1515.
- (28) Freed, J. H. In *Spin Labeling: Theory and Applications*; Berliner, L. J., Ed.; Academic Press: New York, 1976; p 53.
- (29) Schneider, D. J.; Freed, J. H. In *Biological Magnetic Resonance*; Berliner, L. J., Reuben, J., Eds.; Plenum: New York, 1989; p 1.
- (30) Meirovitch, E.; Freed, J. H. *J. Phys. Chem.* **1984**, *88* (21), 4995.
- (31) Polimeno, A.; Freed, J. H. *J. Phys. Chem.* **1995**, *99* (27), 10995.
- (32) Polimeno, A.; Moro, G. J.; Freed, J. H. *J. Chem. Phys.* **1995**, *102* (20), 8094; *Ibid.* **1996**, *104* (3), 1090.
- (33) Sastry, V. S. S.; Polimeno, A.; Crepeau, R. H.; Freed, J. H. *J. Chem. Phys.*, in press.
- (34) Xu, D.; Hall E.; Ober, C. K.; Moscicki, J. K.; Freed, J. H. *J. Phys. Chem.* **1996**, *100*, 15856.
- (35) Gamliel, D.; Freed, J. H. *J. Magn. Reson.* **1990**, *89*, 60.
- (36) Unlike ref 8, we did not fix  $\Delta$  or  $N$  at an average value in the final NLLS fits. In ref 8 all experiments were at the same temperature, for which  $\Delta$  and  $N$  remained the same. In this work we wished to observe their temperature variation. Their inclusion increased somewhat the uncertainty in the fitting parameters due to the correlation among them.<sup>26</sup>
- (37) Hall, E.; Ober, C. K.; Kramer, E. J.; Colby, R. H.; Gillmor, J. R. *Macromolecules* **1993**, *26*, 3764.
- (38) Meirovitch, E.; Nayeem, A.; Freed, J. H. *J. Phys. Chem.* **1984**, *88* (16), 3454.
- (39) Tanaka, H.; Freed, J. H. *J. Phys. Chem.* **1984**, *88* (26), 6633.
- (40) Nayeem, A.; Freed, J. H. *J. Phys. Chem.* **1989**, *93* (17), 6539.
- (41) Shin, Y.-K.; Moscicki, J. K.; Freed, J. H. *Biophys. J.* **1990**, *57*, 445.
- (42) Earle, K. A.; Budil, D. E.; Freed, J. H. *J. Phys. Chem.* **1993**, *97* (50), 13289.
- (43)  $T_m$  observed by ESR is a little greater than the DSC result, probably because the DSC indicated the peak temperature, whereas the ESR spectra showed full alignment only when all the domains underwent the phase transition.
- (44) Speiss and co-workers [Dubinskii, A. A.; Maresch, G. G.; Speiss, H. W. *J. Chem. Phys.* **1994**, *100*, 2437] have used spin-echo methods to study a spin-labeled polymer in the solid state at low temperatures. They employ a field-stepped electron-spin-echo ELDOR method<sup>13,14</sup> which they effectively use in a 2D format. This technique differs from the present 2D-ELDOR based on 2D-FT-ESR methods in that the field-stepped method utilizes highly selective pulses and detection of only the echo maximum rather than our use of nonselective pulses and the collection of the full echo shape. Their technique amounts to a "hole burning" at a particular spectral position, followed by examining its effects on the rest of the spectrum. The 2D-FT-ESR approach, however, involves modern 2D correlation methods, as discussed in the Introduction.<sup>11–16,19–25</sup> Speiss and co-workers use a simple theoretical model to fit their solid-state results. It is very similar to the solid-state spin relaxation "Redfield-type" approach we have utilized in analyzing 2D-FT-ESR experiments on an organic single crystal,<sup>16</sup> and it does not allow for slow motions or precise definitions of ordering. That is, they employ a simple "motional narrowing" theory but in a MOMD format. In our NLLS fits to the MOMD model all motional rates are permitted, but the optimum fits are achieved for values of  $R_{\perp}$  (and  $R$ ) that are in the slow motional regime at the X-band.
- (45) Zannoni, C. In *NMR of Liquid Crystals*; Elmsley, J. W., Ed.; Reidel: Dordrecht, 1985; Chapter 2. Ferrarini, A.; Nordio, P. L.; Moro, G. L.; Crepeau, R. H.; Freed, J. H. *J. Chem. Phys.* **1989**, *91*, 5707.